Microstructure and twinning in epitaxial NiMnGa films

Guido J. Mahnke,[1] M. Seibt,[2,*] and S. G. Mayr[1,†]
[1]*I. Physikalisches Institut, Georg-August-Universität Göttingen, Friedrich-Hund-Platz 1, 37077 Göttingen, Germany*
[2]*IV. Physikalisches Institut, Georg-August-Universität Göttingen, Friedrich-Hund-Platz 1, 37077 Göttingen, Germany*
(Received 3 January 2008; revised manuscript received 3 June 2008; published 3 July 2008)

Although magnetic shape memory alloys have attracted large scientific interest, miniaturization as single-crystalline thin films is still a greatly unresolved issue. In the present work we investigate the microstructure of epitaxial NiMnGa thin films which are fabricated by sputter deposition on magnesium oxide substrates at elevated temperatures. Transmission and scanning electron microscopy as well as atomic force microscopy studies are employed to relate surface topography to twin formation in 7 M martensitic NiMnGa films. Additional findings include pore formation in substrate proximity as well as minor precipitation with reduced nickel and gallium contents.

DOI: 10.1103/PhysRevB.78.012101 PACS number(s): 68.55.−a, 62.20.fg, 81.15.Cd, 81.30.Kf

Since the discovery of large magnetic-field induced strains in NiMnGa bulk crystals by Ullakko *et al.*[1] in 1996, big efforts have been made in order to utilize the so-called magnetic shape memory (MSM) effect for sensors and actuators. In fact, the magnetic shape memory alloy NiMnGa with up to 10% strains reported in the 7 M modulated martensite by Sozinov *et al.*[2] is a promising candidate to fill the gap between piezoelectric actuators with high operation frequencies but low strains and conventional shape memory actuators with large strains but low actuation frequencies. While bulk single-crystal actuators are even commercially available at this time, fabrication of their thin-film counterparts for small devices such as microelectromechanical systems (MEMS) and sensors is still an open issue. Previous work in this area initially focused on polycrystalline NiMnGa thin films, as grown from molecular-beam epitaxy (MBE) (Ref. 3) and sputter deposition.[4] Since then, films produced by pulsed laser deposition,[5] epitaxial growth using MBE,[3,6] and sputtering[7] have also been reported. Yet, the detailed microstructure in thin-film samples has barely been addressed. One previous work, however, discussed possible orientations of twin boundaries in epitaxial NiMnGa on MgO (100) based on diffraction data.[8] Generally the actuation principle of NiMnGa actuators is based on the so-called magnetically induced reorientation (MIR) of twin variants, which requires a martensitic film with twinned microstructure. Epitaxial thin MSM films are generally highly favorable, as they promise maximum strain effects.[9] In the present work we report about epitaxial growth of 7 M martensitic NiMnGa thin film on MgO substrates by sputter deposition and a detailed microstructural analysis by transmission electron microscopy (TEM), scanning electron microscopy (SEM), and atomic force microscopy (AFM), which enables deep insights into the microstructure and macrostructure of twins in the epitaxial film.

Film deposition was performed in a high-vacuum chamber (base pressure of 2×10^{-6} mbar) by sputtering from a $Ni_{49}Mn_{32}Ga_{19}$ (Ref. 10) alloy target with a 2 in. magnetron sputtering gun, as purchased from AJA International. Compositional fine tuning was performed by selectively covering parts of the target with corresponding elemental foils, thus compensating an overall lack of nickel in the deposited films. Using an Ar pressure of 8×10^{-3} mbar and a nominal sputtering power of 21 W (dc) resulted in a deposition rate of 0.125 nm/s. As substrates we utilize epitaxy ready polished 5 mm×25 mm×0.15 mm MgO wafers with (100) orientation, as supplied by Crystec GmbH. These substrates were coated on the backside with a gold reflection layer and clamped on their short side during deposition to enable measurements of growth stresses by a laser beam deflection method, as described before.[11] Details on these stress measurements will be reported elsewhere.[12]

To obtain the desired phases and ordering we use a SiN heating element, attached to the substrate clamp, to reach temperatures of 500–650 °C during deposition. Film preparation is performed after some 300 s of presputtering at ≈42 W sputtering power during which the substrate is covered by a shutter. The sputtering process typically takes a total of 4800 s and results in 600 nm thick layers of NiMnGa with film compositions of 55 at. % Ni, 28 at. % Mn, and 17 at. % Ga, as determined by energy dispersive x-ray spectroscopy (EDX) (based on a film deposited at 500 °C). A deposition temperature of 650 °C results in a reduction in the manganese content by ≈3 at. %, presumably due to its high vapor pressure. After finishing the deposition process, the films cool down to room temperature. Crystal structures are determined using a Bruker D8 Advance x-ray diffractometer equipped with Smart APEX II two-dimensional (2D) charge-coupled device (CCD) detector and Mo K_α radiation. The surface morphology is monitored using a Veeco Nanoscope IV AFM in tapping mode and a Zeiss LEO 35 Supra SEM equipped with EDX system manufactured by the Thermo Electron Corporation. EDX quantification is performed using the Ni, Mn, and Ga K_α lines and an acceleration voltage of 20 kV as proposed in Ref. 13. Additionally TEM microanalyses were performed using a Philips CM200-UT-FEG high-resolution transmission electron microscope (HRTEM) with 200 kV acceleration voltage equipped with Si:Li detector (Oxford Link ISIS) for EDX analysis.

The crystal structure of our thin films was determined to be orthorhombic 7 M,[14,15] based on the (022), (202), and (220) x-ray diffraction spots, which could be identified with the help of calculations with the software "POWDER CELL".[16] No evidence was found that the third diffraction spot might arise from an incomplete martensitic transformation as proposed in Ref. 17 since no remains of the austenite have been

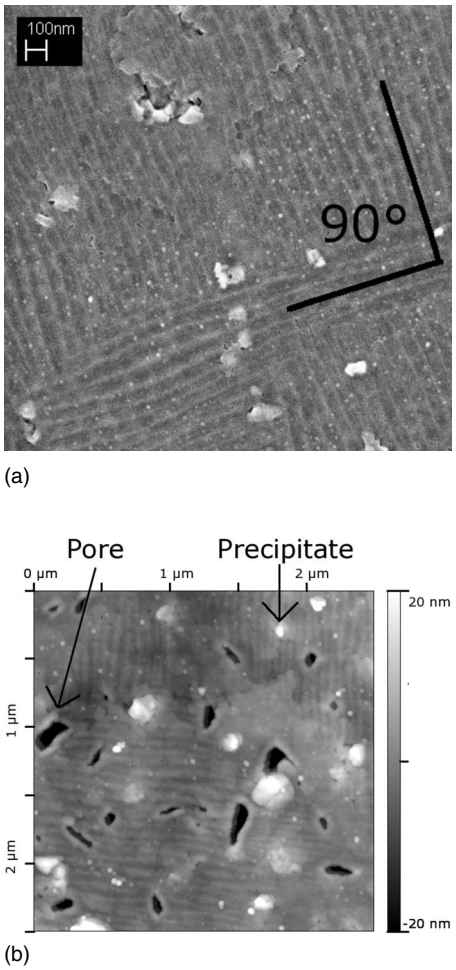

FIG. 1. (a) SEM image showing 90° angles between macrotwin lamellae and (b) AFM topography of the film surface. The perpendicular lamellae intersect either in a zipperlike pattern or perpendicular to each other.

found in the TEM studies. Spotlike diffraction patterns already clearly indicate epitaxial growth of the films on the substrate. On the film surfaces stripe patterns with perpendicular stripes of approximately 20 nm distance could be identified in both SEM and AFM measurements (Fig. 1). SEM images reveal a topography contrasts on the film surface arising from twin lamellae (in the following referred to as "macrotwins") which intersect in an angle of 90°. A similar scenario has already been reported before for bulk NiMnGa.[18] The average distance between the stripes, viz., the width of the twin bands, is determined to be 20 nm by Fast Fourier Transformation (FFT) of an image of a sufficiently large surface area. This is significantly smaller than the corresponding bulk value (some microns),[19] possibly due to substrate constraints and reduced dimensionality of the film geometry. The exact height scale of the stripe pattern is addressed by AFM, which reveals modulations by approximately 5 nm in the z direction. Although slight deviations from straight lines as well as terraces are found, the underlying stripe pattern persists in large areas of the sample.

In addition to that, some fine droplets as well as precipitates and pores can be found on the film surface. The intersections between the macrotwin lamellae are either straight or zipperlike (Fig. 1). The number and size of the pores increase with deposition temperature. For high deposition temperatures >650 °C also the straight lines found in AFM and SEM measurements (Fig. 1) start to buckle or slope.

FIG. 2. Cross-sectional view of a TEM lamella. In a distance of $\approx$50 nm from the substrate a layer of pores can be found. In the center of the image almost horizontal macrotwins are visible, whereas on the right macrotwins in a 45° angle are identified.

For TEM analysis a lamella was cut along a $\langle 110 \rangle$ direction of the MgO substrate by focused ion beam. The cross-sectional view (Fig. 2) indicates macrotwins partially in plane or under angles of 45° and $10° - 12°$ to the substrate. The precipitates which could already be seen in the SEM image were analyzed by EDX to have a composition of 74 at. % Ni, 17 at. % Mn, and 9 at. % Ga whereas we found no significant deviations in composition in the rest of the film—particularly between the 45° stripes and the horizontal stripes (58 at. % Ni, 24 at. % Mn, and 18 at. % Ga in TEM-EDX). A microdiffraction pattern taken for $P2$ shown in Fig. 3 reveals a fcc structure with lattice constant of 0.36 nm. For this reason the precipitates are likely to consist of the γ phase, a disordered, face-centered-cubic phase with the respective lattice constant which has been reported in Ref. 20 to form in NiMnGa for Ni contents higher than 57 at. %. Both precipitates and holes can be seen in Fig. 3. Selected area electron diffraction (SAED) reveals that the film in the vicinity of the precipitates is in the nonmodulated tetragonal phase with (101) twinning planes.

The NiMnGa austenitic phase with a lattice parameter of $a=0.58$ nm is expected to grow with its [100] direction along a [110] direction of the MgO substrate. NiMnGa films with an excess of nickel are known to reside in the martensitic phase at room temperature,[21] viz., the films will undergo

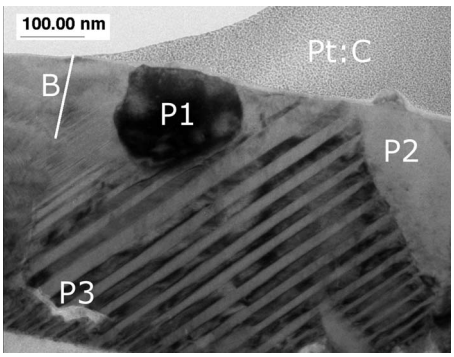

FIG. 3. Bright field image of two precipitates, $P1$ and $P2$, embedded in the twinned microstructure. On the left a boundary B between horizontal and diagonal macrotwins can be seen. On the bottom the twin modulation changes at a pore $P3$. The top of the film is covered by an electron-beam deposited layer of Pt with some C for protection during TEM preparation.

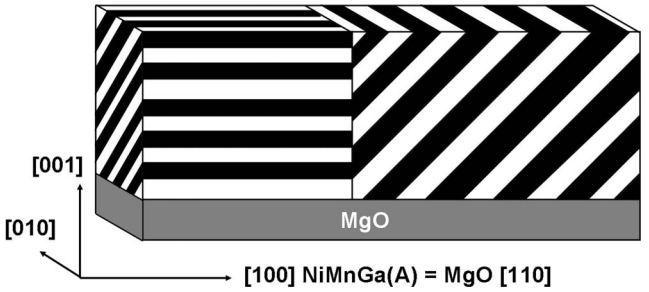

FIG. 4. Schematic drawing of macrotwin lamellea: the MgO {100} plane of the substrate is drawn in gray. When cut along a [110] direction of MgO ([100] of NiMnGa austenite), the NiMnGa twin boundaries of {101} planes can be seen in a 45° angle, while those of {011} planes will appear as straight lines.

a martensitic transformation upon cooling from preparation temperature. Twinning of NiMnGa has been reported to occur on the [110] planes.[22] Therefore six possible twinning planes are expected, four of them in a 45° angle to the substrate and two in a 90° angle. In our TEM studies only twins in 45° angle to the substrate are identified: When MgO is cut along a [110] direction, some of the macrotwins can be seen under a 45° angle but others appear parallel to the substrate. The corresponding geometrical explanation is visualized in Fig. 4. We attribute the slope of the horizontal macrotwin lamellae in the center of Fig. 2 to thickness inhomogeneities and bending of the sample.

About 50 nm apart from the substrate (Fig. 2), pores are identified,[23] which presumably are formed to relief stresses—either during epitaxy or martensitic transformation upon sample cooling. In fact, films produced at higher temperatures even reveal pores throughout the entire film thickness. The film surface itself is covered with an approximately 5 nm thick crystalline layer, as shown in Fig. 5. An EDX line scan (Fig. 5) reveals its predominant nature, viz., manganese oxide.

A 7 M modulated martensitic phase is identified by calculating the FFT of the high-resolution micrograph of a twin lamella. It clearly unveils seven additional diffraction spots between the first-order diffraction spots (see Fig. 6). In the area, where the macrotwins are almost parallel to the surface,

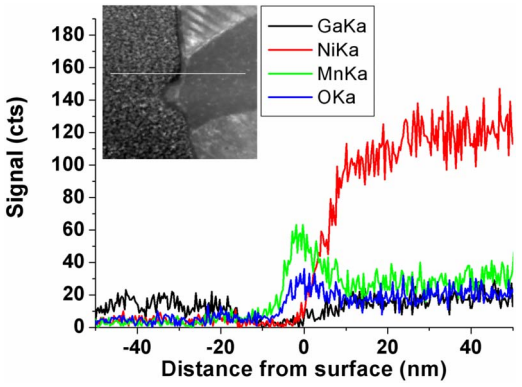

FIG. 5. (Color online) Results of an EDX line scan, which reveals a strong signal for manganese and oxygen but almost no nickel and gallium in the top layer.

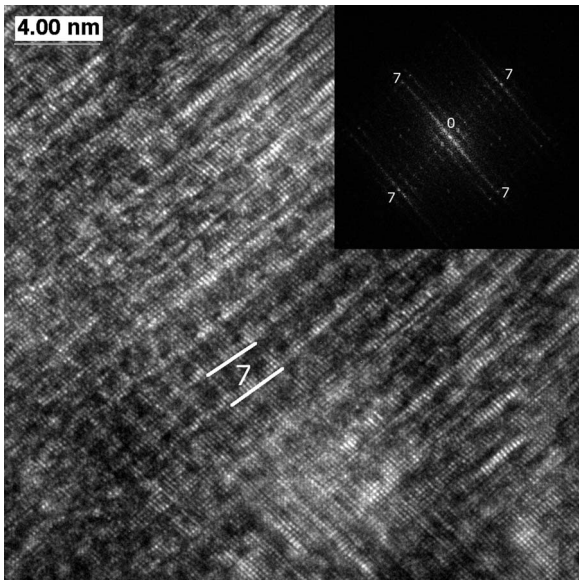

FIG. 6. HRTEM image of a macrotwin and FFT (inset), indicating a 7 M modulated phase by the seven extra spots in the FFT. The modulation is observed in perpendicular directions; the local composition of the film was determined to be 56 at. % Ni, 26 at. % Mn, and 18 at. % Ga.

this modulation can only be seen in every second macrotwin, viz., the modulation direction is different in these macrotwins. For the same reason the incidence angle was not adequate to see the 7 M structure in the 45° macrotwins.

In the following we discuss the physics and consequences of our microstructural characterization of NiMnGa thin films. For all investigated TEM micrographs, no twinning planes in a 90° angle to the substrate plane could be found, which indicates the presence of only four of the six possible twinning scenarios. It is reasonable to attribute this behavior to film stresses due to substrate constraints—primarily within epitaxy and martensitic transformation—causing the twins to be in a 45° angle to the substrate plane ({101} and {011} type). In fact, the formation of twins along {110} is presumably suppressed because these directions lie in the [100] direction of the substrate, in which misfit due to twinning is harder to compensate than in diagonal directions. The macrotwins observed parallel to the substrate plane are likely to be the projections of planes permeating the sample in the viewing direction. The slope of these macrotwins is attributed to inhomogeneous thinning and bending of a lamella. For instance, a slope of 10° can be caused by a thickness change of 17%, which is quite common for cross-sectional TEM samples. In the region of 45° twins, this kind of thickness deviation will not be visible. The macrotwins permeate the whole film, which is expected to be favorable for twin boundary movement. This constitutes one of the necessary conditions for the magnetic shape memory effect formed by reorientation of twin variants, besides the requirement that twinning is not inhibited by substrate constraints. The crystalline top layer of manganese oxide is not too surprising due to our *ex situ* measurements and has been reported before.[24] The cubic crystalline structure has a lattice constant close to 0.45 nm which is typical for cubic manganese oxide. In any

case, the behavior of such an oxide layer, whether it passivates the film and prevents it from further oxidation or growth and blocks twin boundary movement, has to be considered when using NiMnGa for actuators. Precipitates in the film might be blocking twin boundary movement as well, but it is quite likely to get rid of them by adapting deposition parameters (especially deposition temperature and target composition). On the other hand, a mixture of martensitic and γ phase has been reported to improve mechanical properties of the alloy in Ref. 25. The pores in the film require further investigation—their formation is probably stress induced but on the other hand, they might offer a possibility for easy film removal when developing freestanding films for magnetic shape memory applications.

To conclude, we have shown that preparation of fully martensitic epitaxial NiMnGa thin films is possible. Film morphology is dominated by 7 M modulated macrotwins, which permeate the whole film thickness. After exposure to air, the film is covered with a crystalline layer of cubic manganese oxide. Approximately 50 nm apart from the substrate, pores prevail, which are attributed to stress during deposition and martensitic transformation. Generally, the formation of twins is seen in only four of the six possible (100) planes, where one nonzero direction is always perpendicular to the substrate plane. On the film surface different macrotwins intersect in an angle of 90°, while the different variants give rise to a topography contrast. Small precipitates with higher Ni content and different crystal structures were found close to the film surface. Future issues include the impact of microstructure and substrate constraints on magnetically induced movement of twin boundaries, as well as film lift-off, as required for functionalization in thin-film based actuators.

We acknowledge C. Mahn and V. Radisch for technical assistance and preparation of TEM lamellae, H. Klein and H. Sowa for help with x-ray characterization and crystallography, as well as S. Roth (IFW Dreden) for supplying the sputtering target. We also appreciate valuable discussions with T. Edler, I. Kock, and L. Kühnemund. This project is funded by the German DFG—SPP 1239, TP C4.

*Email: seibt@ph4.physik.uni-goettingen.de
†Author to whom correspondence should be addressed; email: smayr@gwdg.de

[1] K. Ullakko, J. K. Huang, C. Kantner, R. C. O'Handley, and V. V. Kokorin, Appl. Phys. Lett. **69**, 1966 (1996).
[2] A. Sozinov, A. A. Likhachev, N. Lanska, and K. Ullakko, Appl. Phys. Lett. **80**, 1746 (2002).
[3] J. Dong, L. Chen, C. Palmstrøm, R. James, and S. McKernan, Appl. Phys. Lett. **75**, 1443 (1999).
[4] M. Ohtsuka and T. Itagaki, Int. J. Appl. Electromagn. Mech. **12**, 49 (2000).
[5] P. Tello, F. Castaño, R. O'Handley, S. Allen, M. Esteve, F. Castaño, A. Labarta, and X. Batlle, J. Appl. Phys. **91**, 8234 (2002).
[6] J. Dong, L. Chen, J. Xie, T. Müller, D. Carr, C. Palmstrøm, S. McKernan, Q. Pan, and R. James, J. Appl. Phys. **88**, 7357 (2000).
[7] G. Jakob and H. Elmers, J. Magn. Magn. Mater. **310**, 2779 (2007).
[8] G. Jakob, T. Eichhorn, M. Kallmayer, and H. J. Elmers, Phys. Rev. B **76**, 174407 (2007).
[9] K. Bhattacharya, A. DeSimone, K. Hane, R. James, and C. Palmstrom, Mater. Sci. Eng., A **273**, 685 (1998).
[10] Composition in at. % based on EDX microanalysis.
[11] S. G. Mayr and K. Samwer, Phys. Rev. Lett. **87**, 036105 (2001).
[12] G. J. Mahnke, Diploma thesis, Göttingen, 2008.
[13] Y. Ge, Ph.D. thesis, Helsinki University of Technology, 2007.
[14] S. Banik *et al.*, Phys. Rev. B **75**, 104107 (2007).
[15] P. Brown, J. Crangle, T. Kanomata, M. Matsumoto, K. Neumann, B. Ouladdiaf, and K. Ziebeck, J. Phys.: Condens. Matter **14**, 10159 (2002).
[16] W. Kraus and G. Nolze, J. Appl. Crystallogr. **29**, 301 (1996).
[17] R. Ranjan, S. Banik, S. R. Barman, U. Kumar, P. Mukhopadhyay, and D. Pandey, Phys. Rev. B **74**, 224443 (2006).
[18] G. Mogylnyy, I. Glavatskyy, N. Glavatska, O. Söderberg, Y. Ge, and V. Lindroos, Scr. Mater. **48**, 1427 (2003).
[19] Q. Pan and R. James, J. Appl. Phys. **87**, 4702 (2000).
[20] Y. Ma, C. Jiang, Y. Li, H. Xu, C. Wang, and X. Liu, Acta Mater. **55**, 1533 (2007).
[21] S. Banik, A. Chakrabarti, U. Kumar, P. K. Mukhopadhyay, A. M. Awasthi, R. Ranjan, J. Schneider, B. L. Ahuja, and S. R. Barman, Phys. Rev. B **74**, 085110 (2006).
[22] V. Martynov and V. Kokorin, J. Phys. III **2**, 739 (1992).
[23] Also based on HRTEM measurements not shown here.
[24] V. Solomon, J. Hong, Y. Tang, A. Berkowitz, and D. Smith, Scr. Mater. **56**, 593 (2007).
[25] Y. Xin, Y. Li, L. Chai, and H. Xu, Scr. Mater. **57**, 599 (2007).